Analytical Uncertainty Quantification for Modal Frequencies with Structural Parameter Uncertainty Using a Gaussian Process Metamodel

Hua-Ping Wan[a,b], Zhu Mao[b], Michael D. Todd[b], Wei-Xin Ren[c,*]

[a] *Department of Civil Engineering, Central South University, Changsha, Hunan Province 410004, China*

[b] *Department of Structural Engineering, University of California, San Diego, 9500 Gilman Dr. 0085, La Jolla, CA 92093-0085, USA*

[c] *Department of Civil Engineering, Hefei University of Technology, Hefei, Anhui Province 230009, China*

Abstract

Quantifying the uncertainty in the dynamic properties of large-scale complex engineering structures presents significant computational challenges. Monte Carlo simulation (MCS) method is extensively employed to perform uncertainty quantification (UQ) because of its generality, stability, and easy implementation. However, a brute-force MCS approach may be unaffordable and impractical when the target model contains a large number of uncertain parameters. In this circumstance, MCS requires a potentially burdensome (if not computationally intractable) number of model evaluations to obtain a credible estimate of the global statistics. In this study, a general framework for analytical UQ of model outputs using a Gaussian process (GP) metamodel is presented, where case inputs are characterized as normal and/or uniform random variables. A detailed derivation of important low-order statistical moments (mean and variance) is given analytically. This analytical method is adopt-

*Corresponding author

Email address: renwx@hfut.edu.cn (Wei-Xin Ren)

ed to characterize the uncertainty of modal frequencies of two bridges with assumed normally- and uniformly-distributed parameters. Meanwhile, the brute-force MCS approach is used for comparison of GP metamodel-derived statistics. Results show that the GP method outperforms the MCS methodology in terms of computational cost, with consistency in the "true" values obtained by MCS. It demonstrates that this GP method is feasible and reliable for modal frequency UQ of complex structures.
Keywords: Uncertainty quantification, Structural dynamics, Modal frequency, Monte Carlo simulation, Gaussian process Metamodel, Bridge structure

1. Introduction

Uncertainty is ubiquitous in all sorts of structural analysis and system identification applications. Specifically, as-built engineering structures are inevitably subjected to many sources of variability, including but not limited to manufacturing-induced geometric tolerances, inherent random variation of materials, imprecisely controlled boundary conditions, load variation, and ambient temperature fluctuation. In the risk assessment community, uncertainties are classified into two categories: *aleatory* and *epistemic*, according to their fundamental essence (Parry (1996)). The former (also termed stochastic, irreducible, or type A uncertainty) is the uncertainty stemming from inherent variation or randomness, whereas the latter (also termed subjective, reducible, or type B uncertainty) is the uncertainty due to incomplete information. Understanding these sources of uncertainty plays an important role in dealing with it, because different types of uncertainty call for different methods of treatment. For a comprehensive understanding of uncertainty sources and the associated management methods, see O'Hagan (2006), Roy and Oberkampf (2011) and Liang and Mahadevan (2011).

The quantification of uncertainty in structural dynamic properties remains an important topic, as such properties are used in a variety of important decision-making applications, such as structural health monitoring, model updating, or test validation/verification. Such dynamic properties include (but aren't necessarily limited to) natural frequencies, mode shapes, the frequency response function (FRF). To obtain more credible predictions for dynamic properties or for proper use in hypothesis testing, the uncertainty present in them should be taken into account. Among these various properties, there is a large body of research work regarding the uncertainty quantification of the FRF. This is due to the fact that FRF has clear physical interpretation and does not require a modal analysis; thus modal parameter identification errors are eliminated. Moreover, FRF data are much more easily accessible than other dynamic properties. The approaches exploited by researchers to characterize uncertainty of the FRF consist of MCS (Farrar et al. (1998)), random matrix theory (Soize (2005)), fuzzy set theory (Moens and Vandepitte (2005)), interval analysis (Moens and Vandepitte (2007)), MCS in conjunction with metamodeling technique (DiazDelaO et al. (2013); Xia and Tang (2013)), statistical modeling approach (Mao and Todd (2013)). Modal frequencies are an indispensable structural dynamic quantity that provides global resonant information about the structure, and because they are relatively easily and robustly measured and relatively low-dimensional, they are often used in the areas of FEM updating (Jaishi and Ren (2005); Ren and Chen (2010); Fang et al. (2012)) and damage identification (Xia et al. (2002)). Modal frequencies also play a critical role in many structural design processes. For example, if the modal frequencies of a pedestrian bridge fall in the range of human movement frequencies, the human-induced vibration will make pedestrians uncomfortable and even cause safety problems. This paper will thus focus on the quantification of modal frequencies where uncertainty is present in the structure. The uncertainties

that have a considerable impact on the modal frequencies include parameter uncertainty, boundary condition variability, and temperature fluctuation. In this work, we restrict our scope on parameter uncertainty, which is the most studied type of uncertainty.

The aforementioned random matrix theory, fuzzy set theory, and interval analysis require the structural stiffness and mass matrices for the subsequent UQ of structural dynamics. For large-scale complex civil structures, they are usually modeled by the high-resolution FEMs involving up to tens or hundreds of millions complex elements with the aid of commercial finite element analysis (FEA) packages, such as ANSYS, ABAQUS and SAP2000. Extracting stiffness and mass matrices from these FEA packages is not an easy task, and multiple iterations between numerical software (e.g., MATLAB) and FEA package will increase computational cost in some degree. The MCS is the most commonly-used and well-known method for uncertainty quantification and propagation. Its robustness depends on neither the type of problem nor resident dimensionality. Furthermore, MCS for UQ also have the advantage of easy implementation. The statistical properties of the model outputs can be obtained by just performing repeated model evaluations using random or pseudo-random numbers to sample from probability distributions of model inputs. However, MCS is extremely time-consuming, because it requires a large number of model evaluations to characterize statistical properties of the model outputs. The behavior of most real structures is simulated by a finite element model (FEM) with a large number of elements (up to tens or hundreds of millions) and complex elements (e.g., solid and shell elements). Thus, when applied to execute UQ tasks for these structures, the brute-force MCS method directly using computationally-expensive FEM will be limited in its applicability due to the high computational cost. For example, in the year 2000, Los Alamos National Laboratory (LANL) in the US quantified the

propagation of uncertainties through a nonlinear FEM simulation of a blast-loaded structure on one of the worlds most powerful computers at that time, Blue Mountain. The analysis took over 72 hours and would have required 17.8 years of equivalent single-processor time (Worden et al. (2005)). Accordingly, the brute-force MCS for UQ is unaffordable and thus unfeasible, especially for the complex physical system.

For the sake of reduction in computational burden, several researchers use the fast-running GP metamodel (also called *Kriging* process) as the surrogate model for the more computationally-expensive simulation of the complex physical system in order to facilitate the daunting task of UQ. DiazDelaO et al. (2013) and Xia and Tang (2013) explore the application of GP metamodel-based MCS for the UQ of FRFs propagated from uncertain parameters. Lockwood et al. (2011) utilize gradient information-assisted GP model (usually known as Gradient-Enhanced Kriging, GEK) to reduce the computational cost associated with MCS for UQ in viscous hypersonic flows. Within GEK framework, Dwight and Han (2009) employ sparse grid integration to perform UQ in Computational Fluid Dynamics (CFD). Using gradient information and prediction uncertainty of GP model, Shimoyama et al. (2013) develop a dynamic adaptive sampling scheme for efficient UQ. Liu and Görtz (2014) combine GEK with Niederreiter sequence based quasi-Monte Carlo (QMC) quadrature to conduct the task of UQ in CFD model subjected to geometric uncertainty. To sum up, these methods all use GP metamodel-based MCS to carry out UQ with computational time reduced, and some of them introduce gradient information, sparse grid integration, dynamic adaptive sampling scheme, or QMC quadrature to further accelerate UQ. This paper proposes an analytical method for UQ of modal frequencies using a GP metamodel, with the specific formulation that the uncertain parameters are either uniformly- or normally-distributed. In the machine learning literature, Girard et al. (2003) have used a GP metamodel with squared

exponential covariance function to make analytical predictions several time steps ahead for normally-distributed uncertain inputs. We adopt and extend Girard et al.'s method, and use a GP metamodel to quantify the uncertainty of modal frequencies from uniformly- and/or normally-distributed parameters. This present analytical GP metamodel approach is more efficient and accurate than GP metamodel-based MCS because it conducts the task of UQ in an analytically integrated manner. It should be pointed out that if the uncertain parameters do not follow (or cannot be modeled with) normal or uniform distributions, using efficient sampling-based MCS method with a GP metamodel is also a promising alternative to alleviate the computational burden associated with UQ drastically.

This paper makes the following main contributions: (1) We develop the analytical GP metamodel-based method for UQ in structural dynamics of cases whose parameters are specified by normal and/or uniform distributions, which are the two most useful (and commonly-used) distributions to characterize parameter uncertainty in the engineering community, absent very domain-specific knowledge. (2) We use the brute-force MCS as a benchmark to verify the feasibility of the proposed method in terms of computational accuracy and efficiency. (3) We explore the relationship between the uncertainty magnitude of individual parameter and the induced overall uncertainty in structural dynamics. Thereby, we can have a good understanding of relative importance of uncertainty magnitude of individual parameter to the uncertainty in structural dynamics.

The rest of this paper is organized as follows. Section 2 outlines the formulation of GP metamodel, and then Section 3 describes the proposed analytical uncertainty quantification using the GP metamodel. The application of the GP approach to UQ of modal frequencies of two real-world bridges is presented in Section 4. Finally, Section 5 concludes this work.

2. Gaussian process metamodel

Gaussian process (GP) (also known as *Kriging* process in the geostatistical literature) metamodel is developed based on concepts of Bayesian statistics. The probabilistic, non-parametric GP model is favored here because of its flexibility in representation of a complex physical system and its ability to quantify the uncertainty associated with its prediction. The flexibility enables a GP metamodel not to be restricted to a certain functional form due to a wide range of covariance functions. The application of GP metamodel to deterministic computer code simulators dates back to the work of Sacks et al. (1989). Recently, there has been an increasing application of GP metamodel in engineering area (e.g., Jones et al. (1998); Simpson et al. (2001); Dwight and Han (2009); Lockwood et al. (2011); Khodaparast et al. (2011); Sankararaman and Mahadevan (2011); Becker et al. (2012); DiazDelaO et al. (2013); Xia and Tang (2013); Shimoyama et al. (2013); Liu and Görtz (2014); Wan and Ren (2014)), and the state of the art may be found in the following references: Mackay (1998), Santner et al. (2003) and Rasmussen and Williams (2006).

2.1. Gaussian process prediction

A process $\{(x_1, f(x_1)), (x_2, f(x_2)), \ldots, (x_n, f(x_n))\}$ is defined as a Gaussian process if any finite number of process members have a joint Gaussian distribution. A GP specified by mean function $\mu(x)$ and covariance function $C(x, x')$ is written as:

$$f(x) \sim \mathcal{GP}\left(\mu(x), C(x, x')\right) \tag{1}$$

As can be seen from Eq. (1), the GP is fully characterized by its mean function and covariance function. Zero mean function is used in this paper due to the fact that we lack prior knowledge of the overall trend of the underlying function (Neal (1998)) and also for the sake of brevity. However, zero mean function does not mean

that the actual function is expected to be close to zero. And the extensively used squared exponential covariance function given below is chosen based on the concept that points close together in the input space should have highly correlated outputs (Bichon et al. (2008)),

$$C(x_i, x_j') = \sigma^2 \exp\left(-\frac{1}{2}\sum_{k=1}^{d}\left(\frac{x_i^k - x_j^k}{\theta_k}\right)^2\right) \tag{2}$$

where $x_i^k(x_j^k)$ is the k-th component of $x_i(x_j)$, and d is the dimension of input space. $\Theta = (\theta_1, \ldots, \theta_d, \sigma^2)$ are the covariance function parameters (usually called hyperparameters), in which θ_i is the length scale measuring how relevant an input is, and σ^2 captures the overall scale of the local correlations.

Consider a training set $\mathcal{D}$ of n cases, $\mathcal{D} = \{(x_1, t_1), (x_2, t_2), \ldots, (x_n, t_n)\}$, in which $x_i = (x_i^1, x_i^2, \ldots, x_i^d)$ is a d-dimensional input vector for case i and t_i is the associated target. Our task is to predict the target t_* at a new input x_*. For the sake of brevity, we rewrite the training data as $\mathcal{D} = (X, T)$, where $X = (x_1^T, x_2^T, \ldots, x_n^T)^T$, and $T = (t_1, t_2, \ldots, t_n)^T$, which follows a joint Gaussian distribution expressed as:

$$p(T) \sim \mathcal{GP}\left(0, C(X, X)\right) \tag{3}$$

And the combination of t_* and training data $\mathcal{D}$, $T_* = (T^T, t_*)^T$, also have a joint Gaussian distribution:

$$p(T_*) \sim \mathcal{GP}\left(0, \begin{bmatrix} C(X, X) & C(X, x_*) \\ C(x_*, X) & C(x_*, x_*) \end{bmatrix}\right) \tag{4}$$

Within the Bayesian framework, the posterior predictive distribution over t_* conditioned on the training data can be calculated from:

$$p(t_*|x_*, \mathcal{D}) = \frac{p(T_*)}{p(T)} \tag{5}$$

Substituting Eq. (3) and Eq. (4) into Eq. (5) yields:

$$p(t_*|x_*, \mathcal{D}) \sim \mathcal{GP}(\hat{t}_*, \nu_{\hat{t}_*}) \tag{6}$$

with the mean and the variance given by:

$$\hat{t}_* = \alpha^T C_* \tag{7}$$

$$\nu_{\hat{t}_*} = \sigma^2 - C_*^T C^{-1} C_* \tag{8}$$

where $C_* = [C(x_*, x_1), C(x_*, x_2), \ldots, C(x_*, x_n)]^T$, $C = C(X, X)$, and $\alpha = C^{-1}T$.

2.2. hyperparameters estimation

The standard conjugate gradient optimization routine is employed to estimate the hyperparameters Θ from training data by maximizing the marginal likelihood, i.e., minimizing negative log marginal likelihood (NLML). It is implemented efficiently due to the fact that both the likelihood and its partial derivatives with respect to the hyperparameters may be calculated analytically. The expression of NLML $\mathcal{L}(\Theta)$ is stated as Eq. (9), and its partial derivatives with respect to each hyperparameter Θ_i is given by Eq. (10) (Rasmussen and Williams (2006)),

$$\mathcal{L}(\Theta) = -\log p(T|X, \Theta) = \frac{1}{2} T^T C^{-1} T + \frac{1}{2} \log |C| + \frac{n}{2} \log(2\pi) \tag{9}$$

$$\frac{\partial \mathcal{L}(\Theta)}{\partial \Theta_i} = \frac{1}{2} \mathrm{tr}\left(C^{-1} \frac{\partial C}{\partial \Theta_i} \right) - \frac{1}{2} T^T C^{-1} \frac{\partial C}{\partial \Theta_i} C^{-1} T \tag{10}$$

where $|\cdot|$ and $\mathrm{tr}(\cdot)$ denote the determinant and trace operator, respectively.

It should be noted that inferring the optimal values of the hyperparameters using a conjugate gradient algorithm may be susceptible to local minima. This means that the obtained hyperparameters Θ are dependent on the chosen initial points. In order to avoid suffering from multiple local optima, the multi-starting point strategy is

utilized in the optimization routine to search the optimal set of hyperparameters. More specifically, first we generate 100 random starting points and compute the NLML values for each case. Then 10 sets of starting points having the smallest NLML values are selected as starting values to carry out conjugate gradient routine. The final optimal set of hyperparameters is the one with the smallest NLML values among these 10 pre-selected cases.

2.3. Model validation

Before the constructed GP model is used as the surrogate model, model accuracy evaluation should be performed to check whether the adopted GP metamodel has enough accuracy. If not, the hyperparameters should be adjusted until the updated GP model has good performance. Considering that GP model has exact predictions over training data for the noise-free condition (i.e., deterministic computer simulation), the residuals can only be obtained using cross-validation technique or an independent data set (Bastos and O'Hagan (2009)). The method of Leave-One-Out Cross-Validation (LOOCV) is implemented in this study for model diagnosis (Jones et al. (1998)).

The i-th cross-validated residual is given by the deviation between predictions at i-th case before and after removing it from training data, i.e., $(t(x_i) - t_{-i}(x_i))$. The standardized cross-validated residual for this observation

$$R_i = \frac{(t(x_i) - t_{-i}(x_i))}{\sqrt{\nu_{-i}(x_i)}} \tag{11}$$

is considered as a diagnostic metric. The normal quantile-quantile (Q-Q) plot is used as the graphic diagnostic for normality test of the residuals $(R_1, R_2, \ldots, R_n)$. If the residual points on normal Q-Q plot are well approximated by a straight line, the normal hypothesis of the residuals is plausible, implying the established GP model is of high quality.

3. Parameter uncertainty quantification

3.1. Methodology

As described previously in Section 1, uncertainty quantification provides a measure of variability in model outputs given uncertainty-involved system inputs. The mean and variance are the two most important order statistics used to quantify the variability. According to probability theory, the mean and variance of output with input probability distribution $p(x_*)$ can be defined as:

$$\begin{aligned} m(t_*) &= \int t_* p(t_*) dt_* \\ &= \int t_* \left(\int p(t_*|x_*, \mathcal{D}) p(x_*) dx_* \right) dt_* \\ &= \int \left(\int t_* p(t_*|x_*, \mathcal{D}) dt_* \right) p(x_*)\ dx_* \end{aligned} \tag{12}$$

$$\begin{aligned} v(t_*) &= \int t_*^2 p(t_*) dt_* - m^2(t_*) \\ &= \int t_*^2 \left(\int p(t_*|x_*, \mathcal{D}) p(x_*) dx_* \right) dt_* - m^2(t_*) \\ &= \int \left(\int t_*^2 p(t_*|x_*, \mathcal{D}) dt_* \right) p(x_*) dx_* - m^2(t_*) \end{aligned} \tag{13}$$

Since

$$\int t_*\, p\left(t_*|x_*, \mathcal{D}\right) dt_* = \hat{t}_* \tag{14}$$

$$\int t_*^2\, p\left(t_*|x_*, \mathcal{D}\right) dt_* = \nu_{\hat{t}_*} + \hat{t}_*^2 \tag{15}$$

and combining the rearrangement of Eq. (7) and Eq. (8) to get

$$\hat{t}_* = \sum_{i=1}^{n} \alpha_i C_{*i} \tag{16}$$

$$\nu_{\hat{t}_*} = \sigma^2 - \sum_{j=1}^{n} \sum_{i=1}^{n} C_{*i} C_{*j} C_{ij}^{-1}, \tag{17}$$

where $C_{*i} = C(x_*, x_i)$, $C_{*j} = C(x_*, x_j)$, $C_{ij} = C(x_i, x_j)$, and α_i is the i-th element of α, we then have mean term given by:

$$\begin{aligned} m(t_*) &= \int \hat{t}_* \, p(x_*) \, dx_* \\ &= \sum_{i=1}^{n} \alpha_i \int C_{*i} \, p(x_*) \, dx_* \\ &= \sum_{i=1}^{n} \alpha_i \gamma_i \end{aligned} \tag{18}$$

and variance term given by:

$$\begin{aligned} v(t_*) &= \int \left(\nu_{\hat{t}_*} + \hat{t}_*^2\right) p(x_*) \, dx_* - m^2(t_*) \\ &= \sigma^2 + \int \left[\left(\sum_{i=1}^{n} \alpha_i C_{*i} \right)^2 - \sum_{j=1}^{n} \sum_{i=1}^{n} C_{*i} C_{*j} C_{ij}^{-1} \right] p(x_*) \, dx_* - m^2(t_*) \\ &= \sigma^2 + \int \left[\sum_{i=1}^{n} \alpha_i C_{*i} \sum_{j=1}^{n} \alpha_j C_{*j} - \sum_{j=1}^{n} \sum_{i=1}^{n} C_{*i} C_{*j} C_{ij}^{-1} \right] p(x_*) \, dx_* - m^2(t_*) \\ &= \sigma^2 + \sum_{j=1}^{n} \sum_{i=1}^{n} \int \left(\alpha_i \alpha_j - C_{ij}^{-1}\right) C_{*i} C_{*j} \, p(x_*) \, dx_* - m^2(t_*) \\ &= \sigma^2 + \sum_{j=1}^{n} \sum_{i=1}^{n} \left(\alpha_i \alpha_j - C_{ij}^{-1}\right) \int C_{*i} C_{*j} \, p(x_*) \, dx_* - m^2(t_*) \\ &= \sigma^2 + \sum_{j=1}^{n} \sum_{i=1}^{n} \left(\alpha_i \alpha_j - C_{ij}^{-1}\right) \Gamma_{ij} - \left(\sum_{i=1}^{n} \alpha_i \gamma_i \right)^2 \end{aligned} \tag{19}$$

In Eq. (18) and Eq. (19), the quantities of γ_i and Γ_{ij} are derived as follows:

$$
\begin{aligned}
\gamma_i &= \int C_{*i}\, p(x_*)\, dx_* \\
&= \sigma^2 \prod_{k=1}^{d} \int \exp\left(-\frac{\left(x_*^k - x_i^k\right)^2}{2\theta_k^2}\right) p\left(x_*^k\right)\, dx_*^k \\
&= \sigma^2 \prod_{k=1}^{d} \sqrt{2\pi}\,\theta_k \int \mathcal{N}_{x_*^k}\left(x_i^k, \theta_k^2\right)\, p\left(x_*^k\right)\, dx_*^k \\
&= \sigma^2 \left(2\pi\right)^{\frac{d}{2}} \prod_{k=1}^{d} \theta_k \int \mathcal{N}_{x_*^k}\left(x_i^k, \theta_k^2\right)\, p\left(x_*^k\right)\, dx_*^k \\
&= \sigma^2 \left(2\pi\right)^{\frac{d}{2}} \prod_{k=1}^{d} \theta_k I_i^k
\end{aligned}
\tag{20}
$$

$$
\begin{aligned}
\Gamma_{ij} &= \int C_{*i} C_{*j}\, p(x_*)\, dx_* \\
&= \sigma^4 \prod_{k=1}^{d} \int \exp\left(-\frac{\left(x_*^k - x_i^k\right)^2}{2\theta_k^2}\right) \exp\left(-\frac{\left(x_*^k - x_j^k\right)^2}{2\theta_k^2}\right) p\left(x_*^k\right)\, dx_*^k \\
&= \sigma^4 \prod_{k=1}^{d} 2\pi\,\theta_k^2 \int \mathcal{N}_{x_*^k}\left(x_i^k, \theta_k^2\right)\, \mathcal{N}_{x_*^k}\left(x_j^k, \theta_k^2\right)\, p\left(x_*^k\right)\, dx_*^k \\
&= \sigma^4 (2\pi)^d \prod_{k=1}^{d} \theta_k^2 \int \mathcal{N}_{x_i^k}\left(x_j^k, 2\theta_k^2\right)\, \mathcal{N}_{x_*^k}\left(\frac{x_i^k + x_j^k}{2}, \frac{\theta_k^2}{2}\right) p\left(x_*^k\right)\, dx_*^k \\
&= \sigma^4 \left(2\pi\right)^d \prod_{k=1}^{d} \theta_k^2\, \mathcal{N}_{x_i^k}\left(x_j^k, 2\theta_k^2\right) \int \mathcal{N}_{x_*^k}\left(\frac{x_i^k + x_j^k}{2}, \frac{\theta_k^2}{2}\right) p\left(x_*^k\right)\, dx_*^k \\
&= \sigma^4 \left(2\pi\right)^d \prod_{k=1}^{d} \theta_k^2\, \phi\left(\frac{x_i^k - x_j^k}{\sqrt{2}\,\theta_k}\right) I_{ij}^k
\end{aligned}
\tag{21}
$$

with

$$
\begin{aligned}
I_i^k &= \int \mathcal{N}_{x_*^k}\left(x_i^k, \theta_k^2\right)\, p\left(x_*^k\right)\, dx_*^k \\
&= \begin{cases} \displaystyle\int \mathcal{N}_{x_*^k}\left(x_i^k, \theta_k^2\right)\, \mathcal{N}_{x_*^k}\left(\mu_k, \sigma_k^2\right)\, dx_*^k & \text{if } x_*^k \sim \mathcal{N}\left(\mu_k, \sigma_k^2\right), \\ \dfrac{1}{(u_k - l_k)} \displaystyle\int \mathcal{N}_{x_*^k}\left(x_i^k, \theta_k^2\right)\, dx_*^k & \text{if } x_*^k \sim \mathcal{U}(u_k, l_k). \end{cases} \\
&= \begin{cases} \phi\left(\dfrac{\mu_k - x_i^k}{\sqrt{\theta_k^2 + \sigma_k^2}}\right) \Big/ \sqrt{\theta_k^2 + \sigma_k^2} & \text{if } x_k \sim \mathcal{N}\left(\mu_k, \sigma_k^2\right), \\ \dfrac{1}{(u_k - l_k)}\left[\Phi\left(\dfrac{u_k - x_i^k}{\theta_k}\right) - \Phi\left(\dfrac{l_k - x_i^k}{\theta_k}\right)\right] & \text{if } x_k \sim \mathcal{U}(u_k, l_k). \end{cases} \\
I_{ij}^k &= \int \mathcal{N}_{x_*^k}\left(\frac{x_i^k + x_j^k}{2}, \frac{\theta_k^2}{2}\right)\, p\left(x_*^k\right)\, dx_*^k \\
&= \begin{cases} \displaystyle\int \mathcal{N}_{x_*^k}\left(\frac{x_i^k + x_j^k}{2}, \frac{\theta_k^2}{2}\right)\, \mathcal{N}_{x_*^k}\left(\mu_k, \sigma_k^2\right)\, dx_*^k & \text{if } x_*^k \sim \mathcal{N}\left(\mu_k, \sigma_k^2\right), \\ \dfrac{1}{(u_k - l_k)} \displaystyle\int \mathcal{N}_{x_*^k}\left(\frac{x_i^k + x_j^k}{2}, \frac{\theta_k^2}{2}\right)\, dx_*^k & \text{if } x_*^k \sim \mathcal{U}(l_k, u_k). \end{cases} \\
&= \begin{cases} \phi\left(\dfrac{2\mu_k - \left(x_i^k + x_j^k\right)}{\sqrt{2\theta_k^2 + 4\sigma_k^2}}\right) \Big/ \sqrt{2\theta_k^2 + 4\sigma_k^2} & \text{if } x_k \sim \mathcal{N}\left(\mu_k, \sigma_k^2\right), \\ \dfrac{1}{(u_k - l_k)}\left[\Phi\left(\dfrac{2u_k - \left(x_i^k + x_i^k\right)}{\sqrt{2}\,\theta_k}\right) - \Phi\left(\dfrac{2l_k - \left(x_i^k + x_i^k\right)}{\sqrt{2}\,\theta_k}\right)\right] & \text{if } x_k \sim \mathcal{U}(l_k, u_k). \end{cases}
\end{aligned}
$$

where $\phi(\cdot)$ and $\Phi(\cdot)$ denote probability density function (PDF) and cumulative distribution function (CDF) of the standard normal distribution, respectively.

The above derivations of quantities of Γ_{ij}, I_i and I_{ij} make use of the identity of Gaussian multiplication, that is, the multiplication of two Gaussian distributions is another Gaussian distribution (but no longer normalized), which is expressed as:

$$
\mathcal{N}_x\left(a, A\right)\, \mathcal{N}_x\left(b, B\right) = z\, \mathcal{N}_x\left(c, C\right)
$$

where

$$C = \left(A^{-1} + B^{-1}\right)^{-1}$$
$$c = C\left(A^{-1}a + B^{-1}b\right).$$
$$z = \mathcal{N}_a\left(b, A + B\right)$$

3.2. Implementation procedure

The present metamodel-based methodology is to analytically evaluate the statistics of the target response of interest with computational time substantially reduced. The core of this methodology is that a GP metamodel is used as the surrogate model of the computationally-expensive finite element simulator. To illustrate this work presented above, a general flowchart for the framework of UQ using a GP metamodel is shown in Fig. 1. This framework involves three main phases as follows:

Phase 1: Prepare training data

The Sobol sequence sampling, a space-filling experimental design, is adopted to prepare training data for establishing the GP metamodel since it has desirable low-discrepancy property (Paskov (1994); Cheng and Druzdzel (2000)). Note that these Sobol points uniformly fall in the d-dimensional unit hypercube $[0, 1]^d$, while the physical parameters of structures follow specific distributions, e.g., normal distribution and uniform distribution. Consequently, before entering inputs into a finite element analysis (FEA) package to obtain the corresponding targets, distribution transformation from sample space to physical space is performed based on the cumulative probability equality principle. Then, to avoid biasing preference to certain variables resulted from different magnitudes among training data, data standardization is carried out before using them to train the GP metamodel. An appropriate way is to normalize inputs/targets to the range $[0, 1]$, or to normalize inputs/targets with zero mean and unit variance. In this paper, for the case that the inputs follow

uniform distribution, we scale inputs to the range $[0, 1]$ and for the case that inputs have normal distribution, we normalize inputs with zero mean and unit variance. For the targets, we make no standardization because we construct GP metamodel for each modal frequency, and thus there is no biasing preference to targets.

Phase 2: Construct Gaussian process metamodel

The conjugate gradient optimization combined with the multi-starting point technique, which attempts to prevent the process from getting trapped in local minima, is adopted to search the most optimal set of hyperparameters. The normal Q-Q graphic diagnostic is launched to verify whether the constructed GP metamodel has acceptably good fitting quality. If not, we repeat the procedure of estimating the hyperparameters until the quality assessment criterion is satisfied.

Phase 3: Uncertainty quantification of model outputs

Two order statistics, mean and variance, can be computed from Eq. (18) and Eq. (19) respectively, within the established GP metamodel. According to the results, we can gain insight into the uncertainty of model outputs of interest propagated from uncertain parameters.

[Fig. 1 about here.]

4. Application

4.1. Case I: Fenghe Bridge

4.1.1. Bridge description

The Fenghe Bridge is a new five-span continuous truss bridge across Baima River in China (Fig. 2). As shown in Fig. 3, the pedestrian bridge is 3.5 m wide and 115 m long, with a center span of 25 m and side spans of 20 m. The superstructures of the pedestrian bridge are mainly made up of four main chords, struts between top and

bottom chords, horizontal and lateral bracings connecting the main chords, wooden deck, and rails. All components of the superstructures, except the deck system and the railing posts, are made of hollow steel tubes. The dimensions of the main chords, struts, horizontal and lateral bracings are $\Phi 273 \times 16\ mm$, $\Phi 140 \times 12\ mm$, $\Phi 114 \times 10\ mm$, respectively. The deck system is composed of hardwoods of dimensions of 3.5 m (length) $\times 0.2$ m (width) $\times 0.15$ m (thickness) uniformly placed at an interval of 0.02 m. The railing posts are welds on the main chords at a distance of 2.2 m.

[Fig. 2 about here.]

[Fig. 3 about here.]

4.1.2. Finite element modeling

The three-dimensional linear elastic FEM for the pedestrian bridge is developed based on the design drawings using FEA package ANSYS. The model has a total of 3035 nodes and 4962 elements, including 4832 beam elements (BEAM44) and 130 mass elements (MASS21). The main modeling aspects are summarized as follows:

- Considering that the wooden deck bolted on the main chords is commonly regarded as a non-structural component, mass elements (MASS21) are used to model the wooden deck.

- The railings, which are usually considered as non-structural components, are sufficiently strong and large that they do contribute to the stiffness, as seen in Fig. 2. Consequently, they are simulated as beam elements (BEAM44) rather than mass elements (MASS21). This concept is verified by the subsequent study.

- The remaining members of the superstructures are all modeled as beam elements (BEAM44).

The resulting FEM and the first four mode shapes are shown in Fig. 4.

[Fig. 4 about here.]

4.1.3. Uncertainty quantification of modal frequencies

In this finite element model, the elastic moduli E of 6 substructures (classified in Tab. 1) are treated as random parameters, although a 210 GPa nominal value is claimed. We assume all parameters are normally distributed, with nominal values as their means and 3% as the coefficient of variation (COV) (ratio of the standard deviation to the mean). Then we will characterize the uncertainty of the first four modal frequencies resulted from pre-characterized random parameters.

[Tab. 1 about here.]

Considering that metamodels will generally fail in their predictive power beyond the range of the training data, it is significant that the training data covers the range of the input space as full as possible. Therefore, a large number of training points are recommended here since this computer-aided experimental method is not restricted by time, place and several limited input values unlike the real-world industrial experiment. In this study, the number of training points generated by Sobol sequence method is set to 300. We found that 300-sample training data hardly increases the computational burden and has good performance as well. Based on the theory stated in Section 3, the resulting mean and standard deviation of the first four modal frequencies are listed in Tab. 2. To investigate the accuracy of the GP method, the MCS approach is utilized to approximate the true values of statistics of modal frequencies. From Fig. 5, we can see that the mean and standard deviation of all four modal frequencies converge at 7.5×10^4 samples. The corresponding results are also listed in Tab. 2. Compared results obtained by GP method and true values

given by MCS method, the largest relative errors of mean and standard deviation are 0.00095% and 0.99132%, respectively. The nearly negligible relative errors verify that the GP method performs as accurate as conventional MCS. However, in terms of computational cost, the analytical GP methodology presents overwhelming superiority over the brute-force MCS. Using the desktop platform of DELL Dimension E520 with Pentium (R) D CPU 2.80 GHz, the former takes 63 minutes (including the time spent in preparing the training data from FEA) whereas the time of the latter is 1667 minutes. Based on the results, we can have a clear picture of how much these uncertain parameters have impact on the first four modal frequencies.

[Tab. 2 about here.]

[Fig. 5 about here.]

Following UQ of modal frequencies, we explore how the uncertainty of modal frequencies is influenced by uncertainty of an individual parameter. The COV of each parameter is taken to be, respectively, 3%, 5%, 10%, 15%, 20%, 25% and 30%, one parameter at a time, and all the rest is fixed to be 3%. The results are shown in Fig. 6. The following observations can be made:

- There is overall trend that with an increase in variation of COV of parameter uncertainty, the uncertainty of modal frequency increases.
- Substructure 2 (four main chords) influences the first four modal frequencies most. This is due to the fact that the four main chords (also called the main truss) constitute the main skeleton of the truss bridge.
- The uncertainty of substructure 6 (railing) also have critical impact on the uncertainty of modal frequencies, especially on the first three ones. It verifies that

railing cannot be treated as non-structural component any more for this truss bridge. The variation in uncertainty of substructure 3 (struts) also leads to the obvious changes in modal frequencies. This can be illustrated by the fact that struts between top and bottom chords improve the overall strength of the bridge.

- The changes of modal frequencies is insensitive to uncertainty change of parameters of the remaining substructures except that the fourth modal frequency exhibits sensitivity to the substructure 1 (supporting tubes). Only when the parameters of these substructures have high degree of uncertainty (COV = 30%) does the magnitude of uncertainty in modal frequencies slightly increase.

[Fig. 6 about here.]

4.2. Case II: Beichuan River Bridge

4.2.1. Bridge description

Another test-bed to validate the GP UQ model is a full-scale half-through concrete-filled steel tubular arch bridge crossing over Beichuan River, as shown in Fig. 7. This 90 m span arch bridge was constructed over the existing old bridge at Xining, China. Fig. 8 shows the elevation and plan of the arch bridge. The superstructure of the arch bridge is composed of a vertical load bearing system, a lateral bracing configuration, and a floor system. Each main rib consists of 4 concrete-filled tubes of the dimensions of $\Phi 650 \times 10$ mm and the depth of main arch rib is 3 m. The main arch ribs and the floor system are vertically connected by 32 suspenders. The floor system comprises the 0.25 m thick concrete slab supported by cross girders at an interval of 5 m. The dimensions of the cross-girder are 21.6 m (length) $\times$ 0.36 m (width) $\times$ 1.361 m (height). The main arch ribs are fixed at two abutments, and connected through 4 pre-stressed strands in the longitudinal direction on each side.

[Fig. 7 about here.]

[Fig. 8 about here.]

4.2.2. Finite element modeling

The arch bridge is modeled in ANSYS environment as a three-dimensional linear elastic model. The arch member, cross girder, and bracing members are modeled by two-node beam elements (BEAM4). Truss elements (LINK10) are used to model all suspenders and pre-stressed tie bars. The arch bridge deck is modeled as shell elements (SHELL63). Solid elements (SOLID45) are employed to simulate the abutments of arch. The connection between the cross-girders and bridge deck is established by using spring element (COMBINE14) with nominal spring stiffness of 5×10^5 N/m in the transverse direction. This FEM consists of 3120 nodes, 1434 beam elements, 564 solid elements, 68 link elements, 1092 shell elements and 288 spring elements. A 3-D sketch of the FEM and the first four mode shapes are given in Fig. 9. For a detailed introduction about this arch bridge and the dynamic analysis, refer to Zong et al. (2005).

[Fig. 9 about here.]

4.2.3. Uncertainty quantification of modal frequencies

For this full-scale engineering structure, a total of 15 parameters (Tab. 3) including material and geometric properties of different components are assumed to be uniformly falling within specified range. Brownjohn and Xia (2000) set the prior parameter uncertainty bounds ±20% to thickness of deck and modulus of steel. Jaishi and Ren (2005) assign ±30% uncertainty bounds to all parameters (e.g., elastic modulus of steel and concrete) except thickness of deck whose uncertainty bounds are set to ±20%. Živanović et al. (2007) set ±30% to the uncertainty bounds of the

modulus of steel, ±20%/±20% to the uncertainty bounds of the thickness of partial deck. Here the ranges of each parameter are set to be ±20% fluctuation with respect to its nominal value. The identical uncertainty bounds selection for all parameters is explained in Subsection 4.3. We will characterize the uncertainty of these 15 parameters to the four modal frequencies, namely the first vertical, second vertical, first torsion and first transverse frequencies (Fig. 9).

[Tab. 3 about here.]

Like the previous example of the truss bridge, a 300-sample training data set created by Sobol sequence sampling methodology is adopted. Applying the GP method to quantify uncertainty of modal frequencies, and the results are tabulated in Tab. 4. MCS method is also used as the metric for accuracy assessment of the GP approach. It can be seen from Fig. 10 that both mean and standard deviation of all four modal frequencies converge at samples of 3.6×10^5. The associated results are visualized in Tab. 4. The largest magnitude of errors in the mean and standard deviation compared to the "true" values approximated by MCS method are 0.12575% and 4.01186%, respectively. The results obtained by the analytical GP method are almost the same as the "true" values, which demonstrates high accuracy of the analytical GP method. In terms of run time, the GP method takes 194 minutes (including the time of generating training data from FEA) while the time of carrying out direct MCS is 64863 minutes.

[Tab. 4 about here.]

[Fig. 10 about here.]

Next we focus on a parametric study of the variation of frequency prediction with respect to parameter uncertainty ranges. The level of uncertainty assigned to

each parameter in turn is: ±20% ,±25% ,±30% ,±35% ,±40% ,±45% and ±50% respectively, and uncertainty range of the remaining parameters keeps constant (i.e., ±20%). The results are presented in Fig. 11, from which the observations are reported as follows:

- Uncertainty of modal frequency increases monotonically with increasing level of uncertainties in most of the parameters. However, sometimes the increase of uncertainty of parameter 15 leads to a reduction of uncertainty of the second vertical modal frequency. This phenomenon implies that the second modal frequency becomes less spread out over the larger range of parameter 15.

- For the first vertical modal frequency, its uncertainty significantly grows as the levels of uncertainty of parameters 1, 2, 4, 5, 9 and 10 increase. The increase in the size of uncertainty of parameters 1, 2, 4, 5, 9, 10, 11 and 12 result in larger uncertainty in the second vertical modal frequency. As the uncertainty levels of parameters 1, 2, 4, 5 and 15 become higher, the magnitudes of uncertainty of the first torsion modal frequency escalate. And for the first transverse modal frequency, only the increase of uncertainty of parameters 4, 5 and 15 can lead to the dramatic increasing uncertainty.

- The uncertainty of these four modal frequencies is all sensitive to the variation of parameters 4 and 5 and is insensitive to parameter 14. Some parameters that have little impact on the uncertainty of one modal frequency can considerably influence other modal frequencies. For example, the increasing uncertainty of parameter 15 has negligible effect on the uncertainty of the first vertical modal frequency but cause the higher uncertainty of the first transverse modal frequency. The higher the uncertainty of the parameter 9, the higher the uncertainty of the second modal frequency while that of the first vertical modal frequency has little change.

[Fig. 11 about here.]

4.3. Discussion

This section presents two complex engineering examples, one truss bridge and one arch bridge, to verify the feasibility of applying GP method to quantify the uncertainty of the modal frequencies. To cover two scenarios of parameter uncertainty (normal and uniform distributions), the parameters of the truss bridge and arch bridge are assumed as normally and uniformly distributed, respectively. For the truss bridge, we assume the uncertain parameters with the same COV, and for the arch bridge, the bounds of each parameter are set to be the same percentage change with respect to its nominal value. The assumption of the same type of uncertainty and the same magnitude of uncertainty in each structure aims at distinguishing the importance or impact of these uncertain parameters under equal conditions (i.e., the identical range of uncertainty) in the subsequent sensitivity analysis of magnitude changes of parameter uncertainty. Fig. 12 is used to explain this selected assumption of identical uncertainty. Assume the prior uncertainty bounds are 20% for parameter 1 and 10% for parameter 2, and the uncertainty percentage changes are set to 10%, 15%, 20%, and 25%. The sensitivity analysis of parameter uncertainty magnitude graph is plotted when uncertainty percentage changes are assigned to each parameter in turn and other parameter uncertainty level keep constant. Therefore the black line for parameter 1 is corresponding to the dots: (10%, 10%), (15%, 10%), (20%, 10%), (25%, 10%) and the red line for parameter 2 is corresponding to the dots: (20%, 10%), (20%, 15%), (20%, 20%), (20%, 25%). From the Fig. 12, we can conclude that uncertainty of parameter 2 (red line) more affect the overall uncertainty and then is more important. Yet, this conclusion is very controversial because this larger variation of standard deviation can result from larger uncertainty bounds of

both parameters not just from one parameter's uncertainty level change (see the dots behind the lines). That is why we adopt identical prior uncertainty bounds for all parameters.

[Fig. 12 about here.]

For the quantification of the uncertainty in quantity of interest propagated from uncertain parameters, it is known that prior parameter uncertainty dominates the final results. Accordingly, special care must be taken to choose prior parameter uncertainty that characterized by ranges and/or distributions. As far as authors are concerned, the strategies of determining prior parameter uncertainty are primarily composed of following two aspects. (1) Prior parameter uncertainty should represent the available information from measurement or observations. For example, it may be reasonable to model prior parameter uncertainty as uniform distribution when lower and upper bounds of the parameter are known, or as normal distribution when mean and standard deviation of the parameter are known. (2) Structural parameters including material and geometric parameters should follow the physical constraint of positive definiteness and engineering judgment. When normal distribution is used to specify parameter uncertainty, the value of COV should be small enough to guarantee that almost all samples spread in the positive range. For the scenario with the largest COV=30% in the first case, the normalized 99.9% tolerance interval is [1-3.29×0.3, 1+3.29×0.3], which are positive. Engineering judgment refers to engineering common sense. For example, material parameters usually have higher level of uncertainty than geometric parameters.

This proposed analytical GP metamodel-based method is suitable for the cases whose parameters follow normal and/or uniform distributions, both of which are commonly utilized to characterize the parametric uncertainty in engineering com-

munity. For the cases whose parameters are specified by other distributions, MCS in combined with GP metamodel is still an appealing means to deal with these UQ problems. Alternatively, to accelerate the convergence of MCS, we can adopt the more efficient sampling methods, e.g., Quasi-Monte Carlo methods and Latin hypercube sampling.

5. Conclusion and summary

This work presents a framework for uncertainty quantification and propagation using an analytical method by GP metamodel when uncertain inputs follow normal and/or uniform distributions. Normal and uniform distributions are the two most useful (and commonly-used) distributions used to characterize parameter uncertainty in engineering community. For real-world structures, models are often complex and high dimensional. Accordingly, when computing resources are limited, uncertainty evaluation of structural dynamics of these structures using brute-force MCS approach will suffer from a computational bottleneck. This analytical GP approach can quantify uncertainty of model outputs efficiently and accurately, thus circumventing the problem of severe computational cost. This analytical GP approach is applied to characterize the uncertainty of modal frequencies of the full-scale truss and arch bridges propagated from uncertain parameters. And MCS approach is used as the benchmark to check the accuracy of the GP method. Results show that the GP methodology is as accurate as conventional methodology, but also offers considerable computational savings. Therefore, the GP metamodel replacing the complex numerical model is a good alternative to carry out the computationally-intensive task of UQ of structural dynamics. In this paper, we also investigate the relationship between the uncertainties of modal frequencies and parameters for two bridges

with different parameter uncertainty characteristics. The following conclusions may be drawn:

- The notion that increases in input parameter uncertainty will increase the uncertainty of modal frequencies is not always true (see Fig. 11 (b)). That is to say, the relationship between uncertainties of modal frequencies and input parameters is not necessarily monotonically increasing. If the function $f(x)$, denoting the relationship between modal frequency and parameters, oscillates sharply at small range of x and become steady as the range of x increases, the increase in uncertainty of parameters will result in a reduction in uncertainty of modal frequency instead.

- When the structure is more complex and has huge number of uncertain parameters (e.g., the arch bridge) and there is no credible expert prior or existing information, it is hard to determine the uncertainty level of which parameters most significantly affect the uncertainty of modal frequencies. Depicting the relationship plot of uncertainty of modal frequencies versus that of parameters can enable us to gain insight into the internal mechanism. For example, the results verify our previous intuitive judgment that the railing cannot be considered as non-structural component for this truss bridge in finite element modeling because its uncertainty has great impact on the modal frequencies.

- The influences of uncertainty of parameters on uncertainty in different order modal frequencies, especially the mode of different classes (e.g., vertical, torsion modes), are sometimes greatly different, such as parameters 9 (density of deck) and 15 (spring stiffness in lateral direction) of the arch bridge. It tells us that we should pay close attention to those parameters whose uncertainties have little influence on certain modal frequencies but can affect other modal frequencies more.

Acknowledgement

The first author would like to acknowledge support from the China Scholarship Council (CSC) through Grant 201206370090.

References

1. Parry, G.W.. The characterization of uncertainty in probabilistic risk assessments of complex systems. *Reliability Engineering & System Safety* 1996;**54**(2-3):119–126.

2. O'Hagan, A.. Bayesian analysis of computer code outputs: A tutorial. *Reliability Engineering & System Safety* 2006;**91**(10-11):1290–1300.

3. Roy, C.J., Oberkampf, W.L.. A comprehensive framework for verification, validation, and uncertainty quantification in scientific computing. *Computer Methods in Applied Mechanics and Engineering* 2011;**200**(25-28):2131–2144.

4. Liang, B., Mahadevan, S.. Error and uncertainty quantification and sensitivity analysis in mechanics computational models. *International Journal for Uncertainty Quantification* 2011;**1**(2):147–161.

5. Farrar, C.R., Doebling, S.W., Cornwell, P.J.. A comparison study of modal parameter confidence intervals computed using the Monte Carlo and Bootstrap techniques. In: *Proceedings of SPIE—the International Society for Optical Engineering*; vol. 2. 1998, p. 936–944.

6. Soize, C.. A comprehensive overview of a non-parametric probabilistic approach of model uncertainties for predictive models in structural dynamics. *Journal of Sound and Vibration* 2005;**288**(3):623–652.

7. Moens, D., Vandepitte, D.. A fuzzy finite element procedure for the calculation of uncertain frequency-response functions of damped structures: Part 1—procedure. *Journal of Sound and Vibration* 2005;**288**(3):431–462.

8. Moens, D., Vandepitte, D.. Interval sensitivity theory and its application to frequency response envelope analysis of uncertain structures. *Computer Methods in Applied Mechanics and Engineering* 2007;**196**(21-24):2486–2496.

9. DiazDelaO, F.A., Adhikari, S., Saavedra Flores, E.I., Friswell, M.I.. Stochastic structural dynamic analysis using Bayesian emulators. *Computers & Structures* 2013;**120**:24–32.

10. Xia, Z., Tang, J.. Characterization of dynamic response of structures with uncertainty by using Gaussian processes. *Journal of Vibration and Acoustics* 2013; **135**(5):051006.

11. Mao, Z., Todd, M.. Statistical modeling of frequency response function estimation for uncertainty quantification. *Mechanical Systems & Signal Processing* 2013; **38**(2):333–345.

12. Jaishi, B., Ren, W.X.. Structural finite element model updating using ambient vibration test results. *Journal of Structural Engineering* 2005;**131**(4):617–628.

13. Ren, W.X., Chen, H.B.. Finite element model updating in structural dynamics by using the response surface method. *Engineering Structures* 2010;**32**(8):2455–2465.

14. Fang, S.E., Ren, W.X., Perera, R.. A stochastic model updating method for parameter variability quantification based on response surface models and Monte Carlo simulation. *Mechanical Systems & Signal Processing* 2012;**33**:83–96.

15. Xia, Y., Hao, H., Brownjohn, J.M.W., Xia, P.Q.. Damage identification of structures with uncertain frequency and mode shape data. *Earthquake Engineering & Structural Dynamics* 2002;**31**(5):1053–1066.

16. Worden, K., Manson, G., Lord, T.M., Friswell, M.I.. Some observations on uncertainty propagation through a simple nonlinear system. *Journal of Sound and Vibration* 2005;**288**(3):601–621.

17. Lockwood, B., Rumpfkeil, M., Yamazaki, W., Mavriplis, D.. *Uncertainty quantification in viscous hypersonic flows using gradient information and surrogate modeling*. Aerospace Sciences Meetings. American Institute of Aeronautics and Astronautics; 2011, .

18. Dwight, R.P., Han, Z.H.. *Efficient uncertainty quantification using Gradient-Enhanced Kriging*. Structures, Structural Dynamics, and Materials and Co-located Conferences. American Institute of Aeronautics and Astronautics; 2009, .

19. Shimoyama, K., Kawai, S., Alonso, J.J.. *Dynamic adaptive sampling based on Kriging surrogate models for efficient uncertainty quantification*. Structures, Structural Dynamics, and Materials and Co-located Conferences. American Institute of Aeronautics and Astronautics; 2013, .

20. Liu, D., Görtz, S.. *Efficient quantification of aerodynamic uncertainty due to random geometry perturbations*; vol. 124 of *Notes on Numerical Fluid Mechanics and Multidisciplinary Design*; book section 7. Springer International Publishing; 2014, p. 65–73.

21. Girard, A., Rasmussen, C.E., Quinonero-Candela, J., Murray-Smith, R.. Gaussian

Process priors with uncertain inputs—Application to multiple-step ahead time series forecasting. Cambridge: MIT Press. ISBN 0262025507; 2003, .

22. Sacks, J., Welch, W.J., Mitchell, T.J., Wynn, H.P.. Design and analysis of computer experiments. *Statistical Science* 1989;**4**(4):409–423.

23. Jones, D., Schonlau, M., Welch, W.. Efficient global optimization of expensive black-box functions. *Journal of Global Optimization* 1998;**13**(4):455–492.

24. Simpson, T.W., Mauery, T.M., Korte, J.J., Mistree, F.. Kriging models for global approximation in simulation-based multidisciplinary design optimization. *AIAA journal* 2001;**39**(12):2233–2241.

25. Khodaparast, H.H., Mottershead, J.E., Badcock, K.J.. Interval model updating with irreducible uncertainty using the Kriging predictor. *Mechanical Systems and Signal Processing* 2011;**25**(4):1204–1226.

26. Sankararaman, S., Mahadevan, S.. Model validation under epistemic uncertainty. *Reliability Engineering & System Safety* 2011;**96**(9):1232–1241.

27. Becker, W., Oakley, J.E., Surace, C., Gili, P., Rowson, J., Worden, K.. Bayesian sensitivity analysis of a nonlinear finite element model. *Mechanical Systems and Signal Processing* 2012;**32**:18–31.

28. Wan, H.P., Ren, W.X.. Parameter selection in Finite-Element-Model updating by global sensitivity analysis using Gaussian process metamodel; 2014. DOI: 10.1061/(ASCE)ST.1943-541X.0001108.

29. Mackay, D.J.C.. *Introduction to* Gaussian processes. NATO ASI Series. Kluwer Academic; 1998, p. 133–166.

30. Santner, T.J., Williams, B.J., Notz, W.I.. *The design and analysis of computer experiments*. New York: Springer; 2003.

31. Rasmussen, C.E., Williams, C.K.I.. Gaussian processes for machine learning. MIT Press; 2006.

32. Neal, R.M.. *Regression and classification using Gaussian process priors*. Oxford University Press; 1998, p. 475–501.

33. Bichon, B., Eldred, M., Swile, L., Mahadevan, S., McFarland, J.. Efficient global reliability analysis for nonlinear implicit performance functions. *AIAA journal* 2008;**46**(10):2459–2468.

34. Bastos, L.S., O'Hagan, A.. Diagnostics for Gaussian process emulators. *Technometrics* 2009;**51**(4):425–438.

35. Paskov, S.. Computing high dimensional integrals with applications to finance. Report Technical Report CUCS-023-94; Department of Computer Science, Department of Computer Science; 1994.

36. Cheng, J., Druzdzel, M.J.. Computational investigation of low-discrepancy sequences in simulation algorithms for bayesian networks. In: *Proceedings of the Sixteenth Conference on Uncertainty in Artificial Intelligence*. Morgan Kaufmann Publishers; 2000, p. 72–81.

37. Zong, Z.H., Jaishi, B., Ge, J.P., Ren, W.X.. Dynamic analysis of a half-through concrete-filled steel tubular arch bridge. *Engineering Structures* 2005;**27**(1):3–15.

38. Brownjohn, J., Xia, P.. Dynamic assessment of curved cable-stayed bridge by model updating. *Journal of Structural Engineering* 2000;**126**(2):252–260.

39. Živanović, S., Pavic, A., Reynolds, P.. Finite element modelling and updating of a lively footbridge: The complete process. *Journal of Sound and Vibration* 2007; **301**(1-2):126–145.

List of Figures

List of Tables

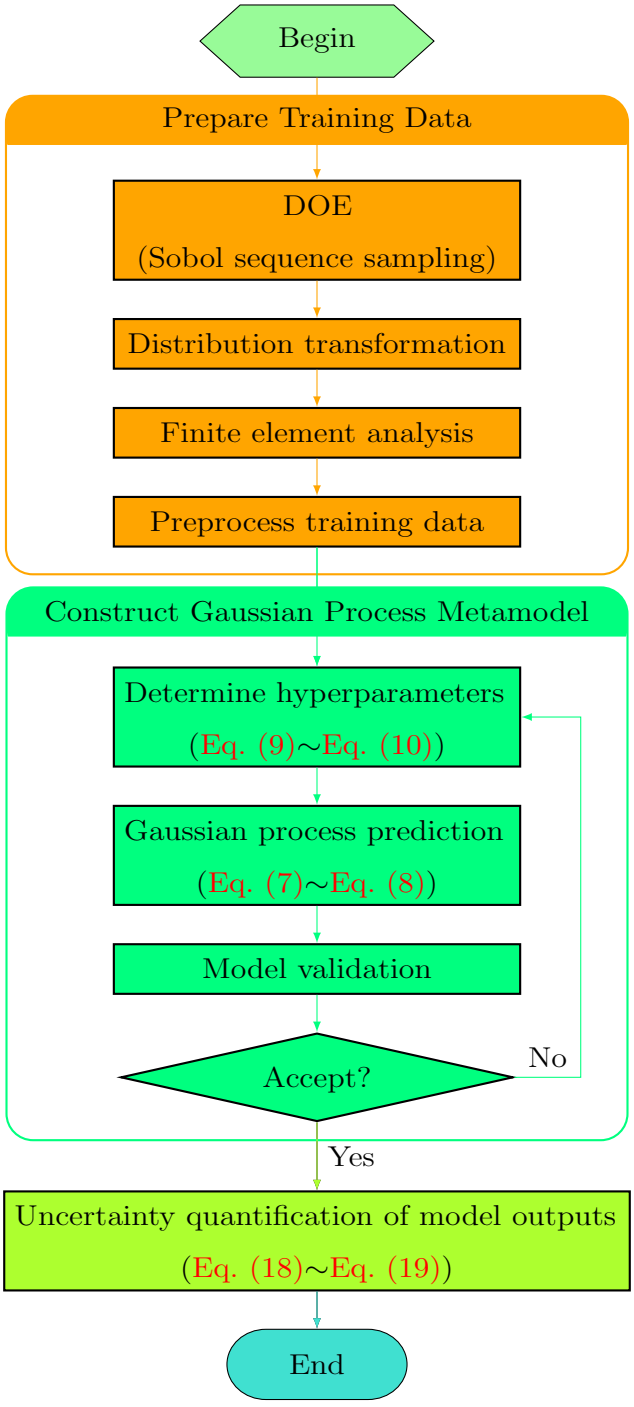

Fig. 1. Flowchart of uncertainty quantification based on Gaussian process metamodel.

Fig. 2. Overview of the Fenghe Bridge.

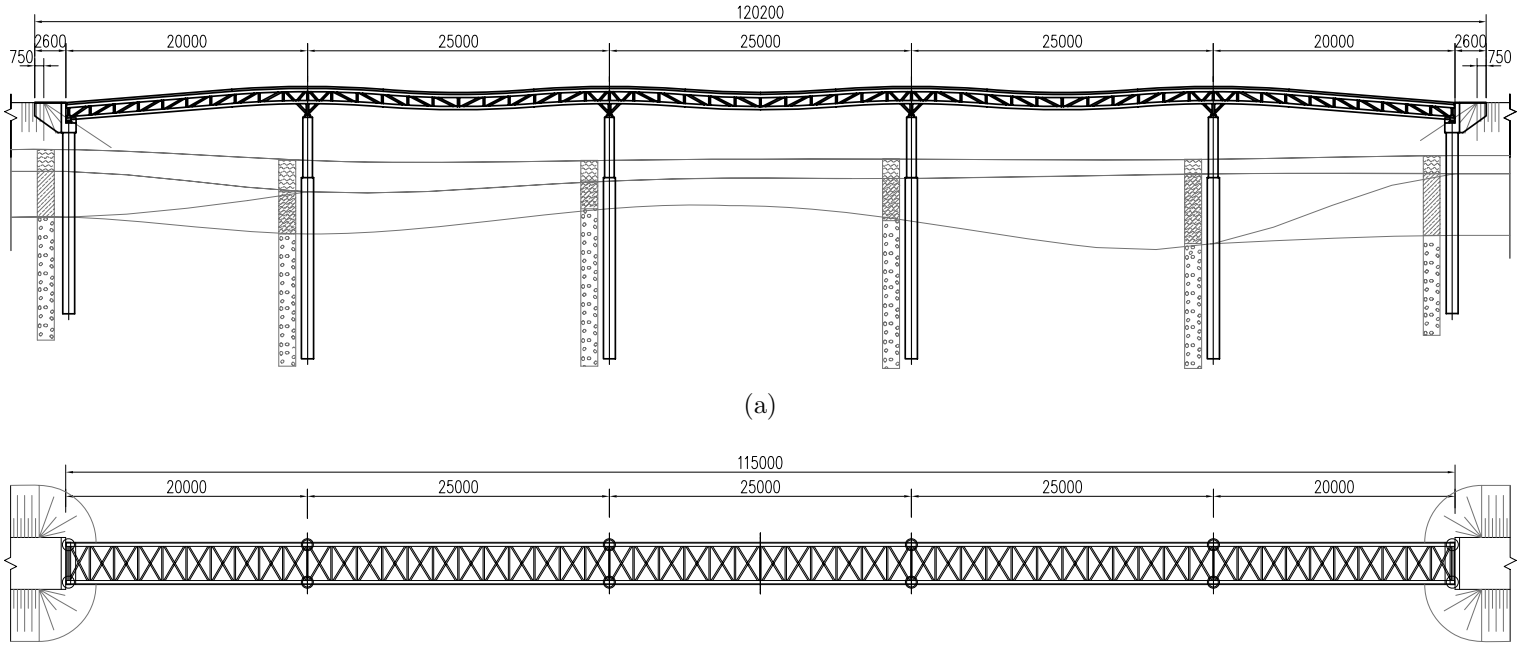

Fig. 3. Configuration of the Fenghe Bridge: (a) Elevation and (b) Plan (unit: mm).

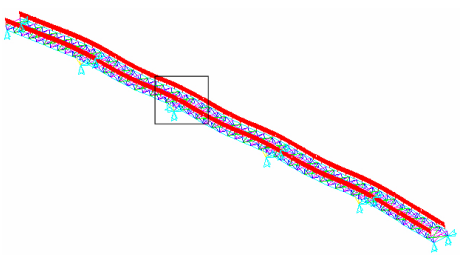

Overview

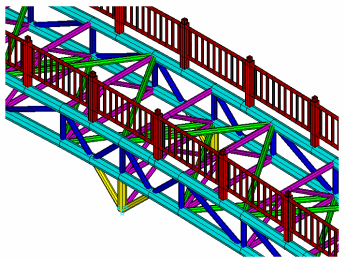

Zoom region

(a)

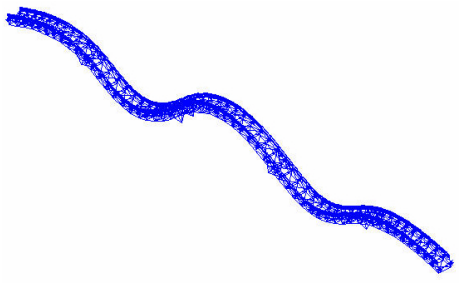

First vertical mode

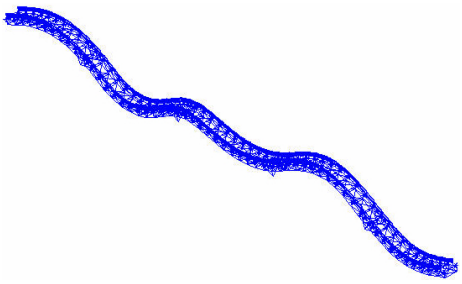

Second vertical mode

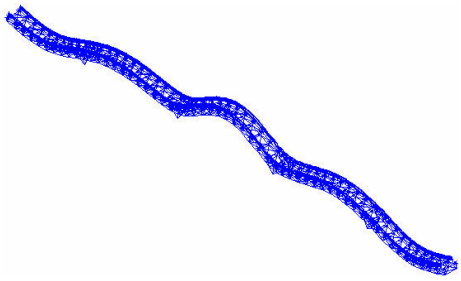

Third vertical mode

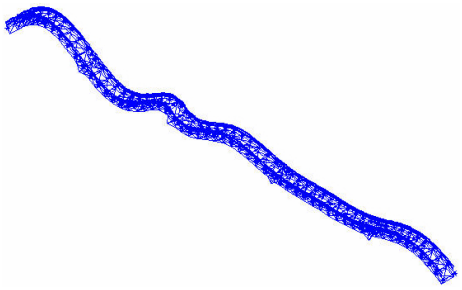

Fourth vertical mode

(b)

Fig. 4. FEM and mode shapes of the Fenghe Bridge: (a) FEM and (b) Mode shapes.

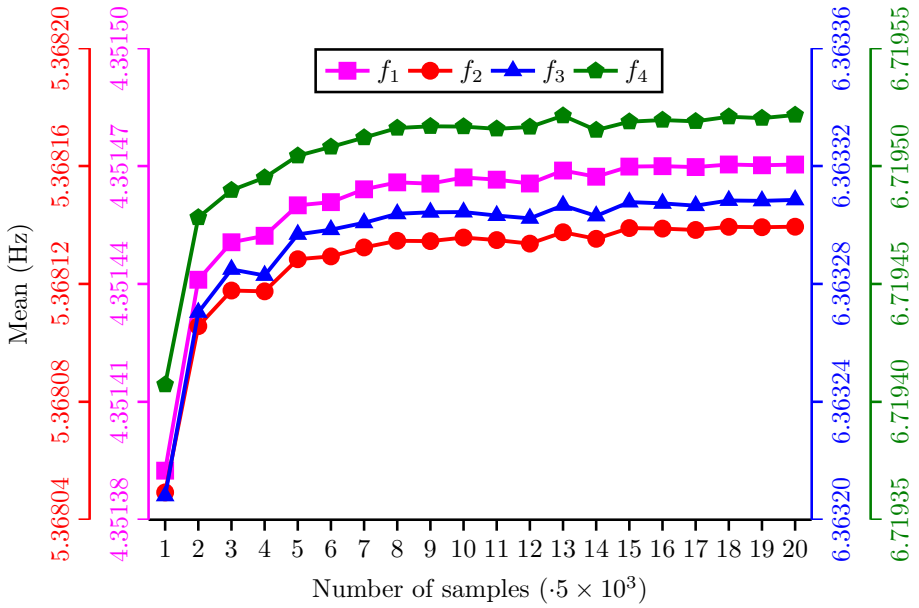

(a)

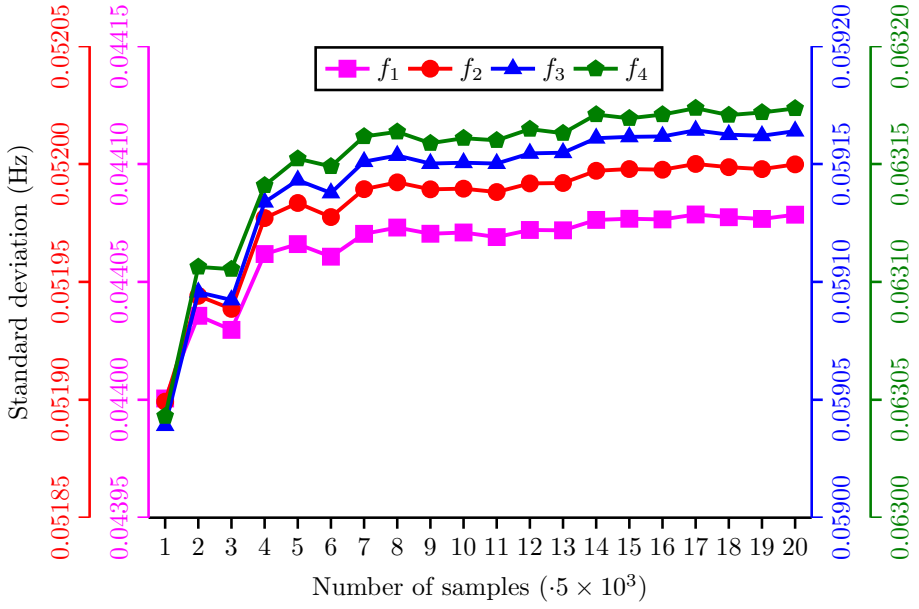

(b)

Fig. 5. Mean and standard deviation of modal frequencies of the Fenghe Bridge versus number of samples based on MCS: (a) Mean and (b) Standard deviation.

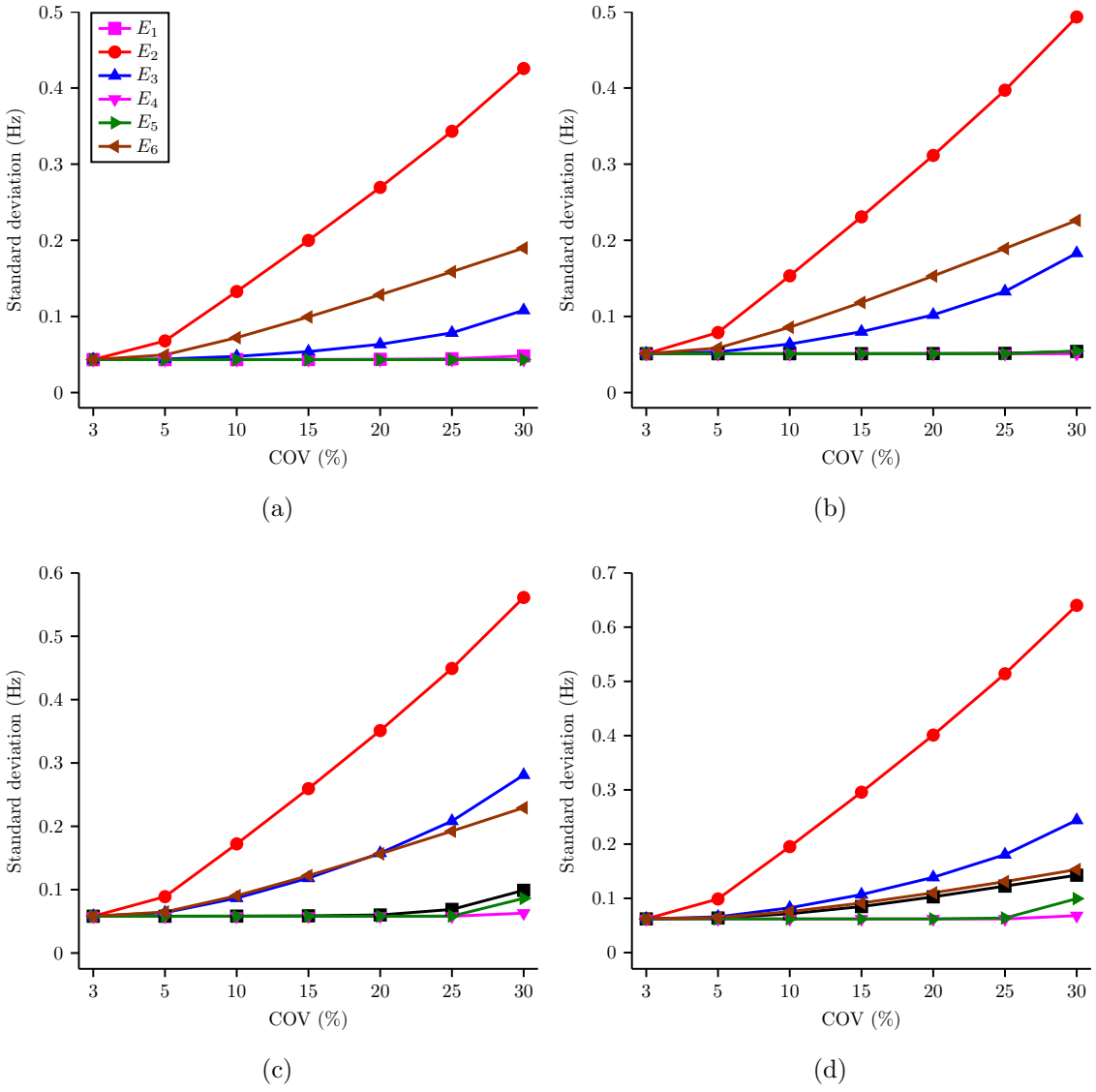

Fig. 6. Standard deviation of modal frequencies of the Fenghe Bridge versus COV: (a) f_1, (b) f_2, (c) f_3 and (d) f_4.

Fig. 7. General view of the Beichuan River Bridge.

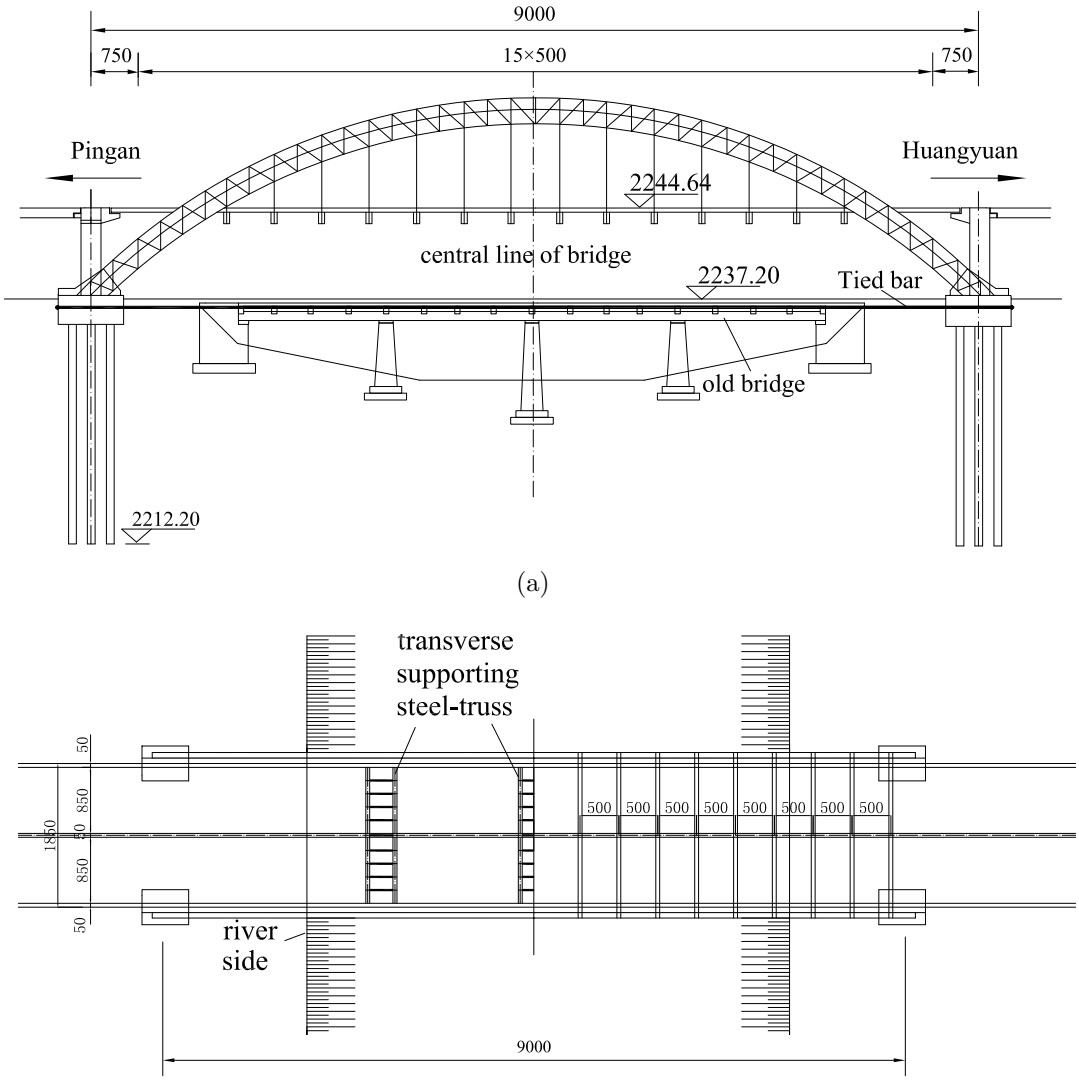

Fig. 8. Configuration of the Beichuan River Bridge: (a) Elevation and (b) Plan (unit: cm).

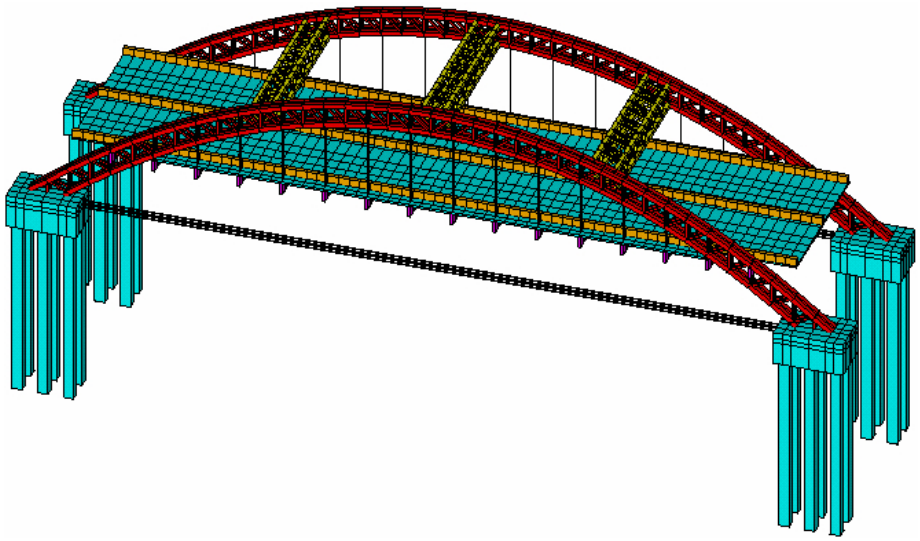

Overview

(a)

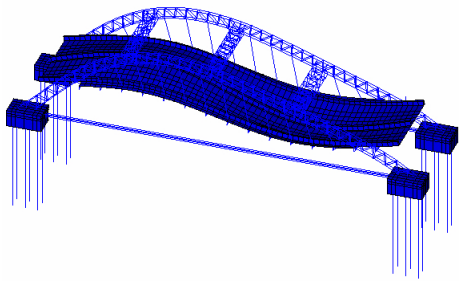

First vertical mode

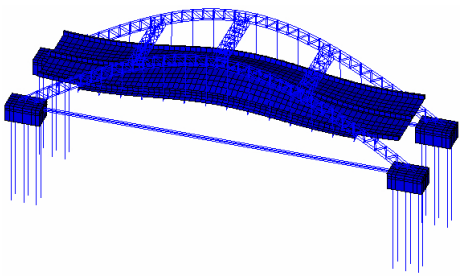

Second vertical mode

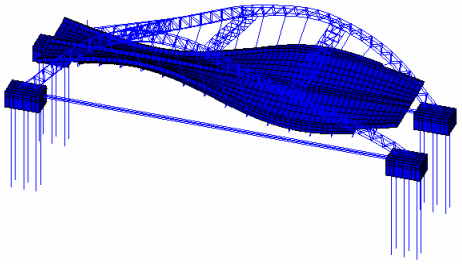

First torsion mode

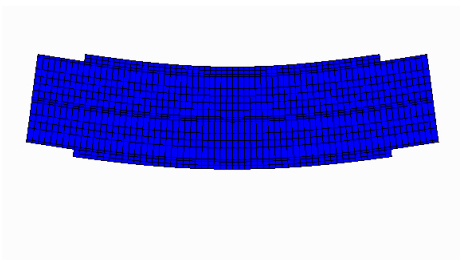

First transverse mode

(b)

Fig. 9. FEM and mode shapes of the Beichuan River Bridge: (a) FEM and (b) Mode shapes.

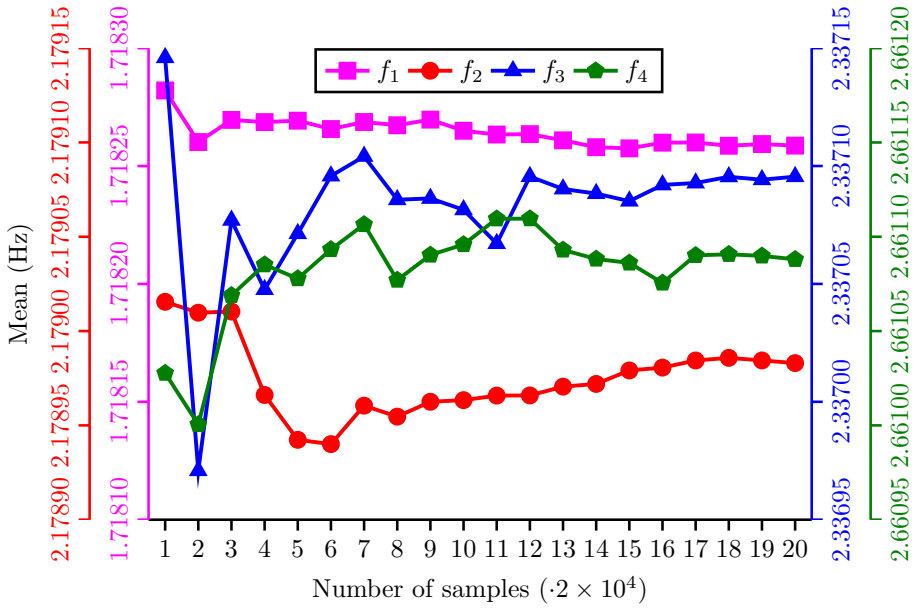

(a)

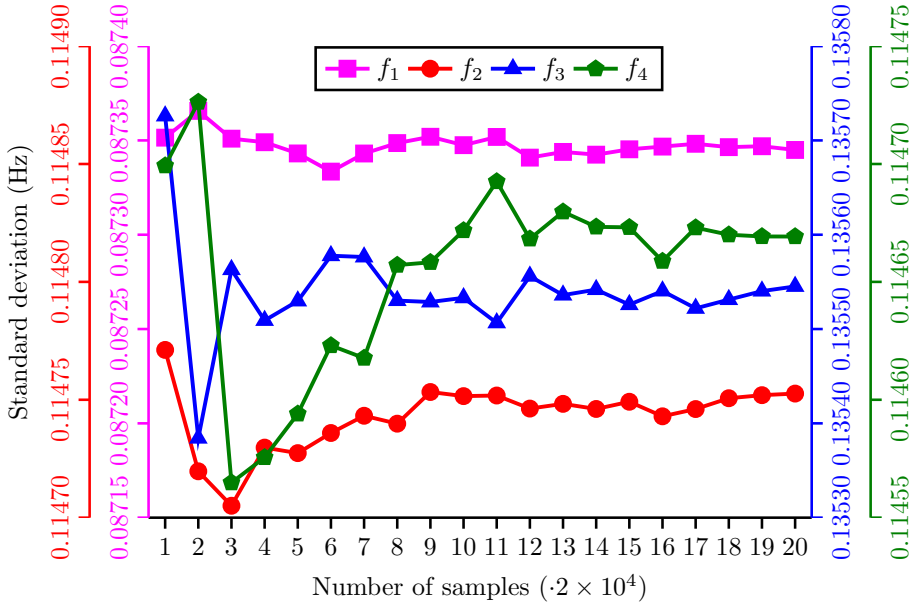

(b)

Fig. 10. Mean and standard deviation of modal frequencies of the Beichuan River Bridge versus number of samples based on MCS: (a) Mean and (b) Standard deviation.

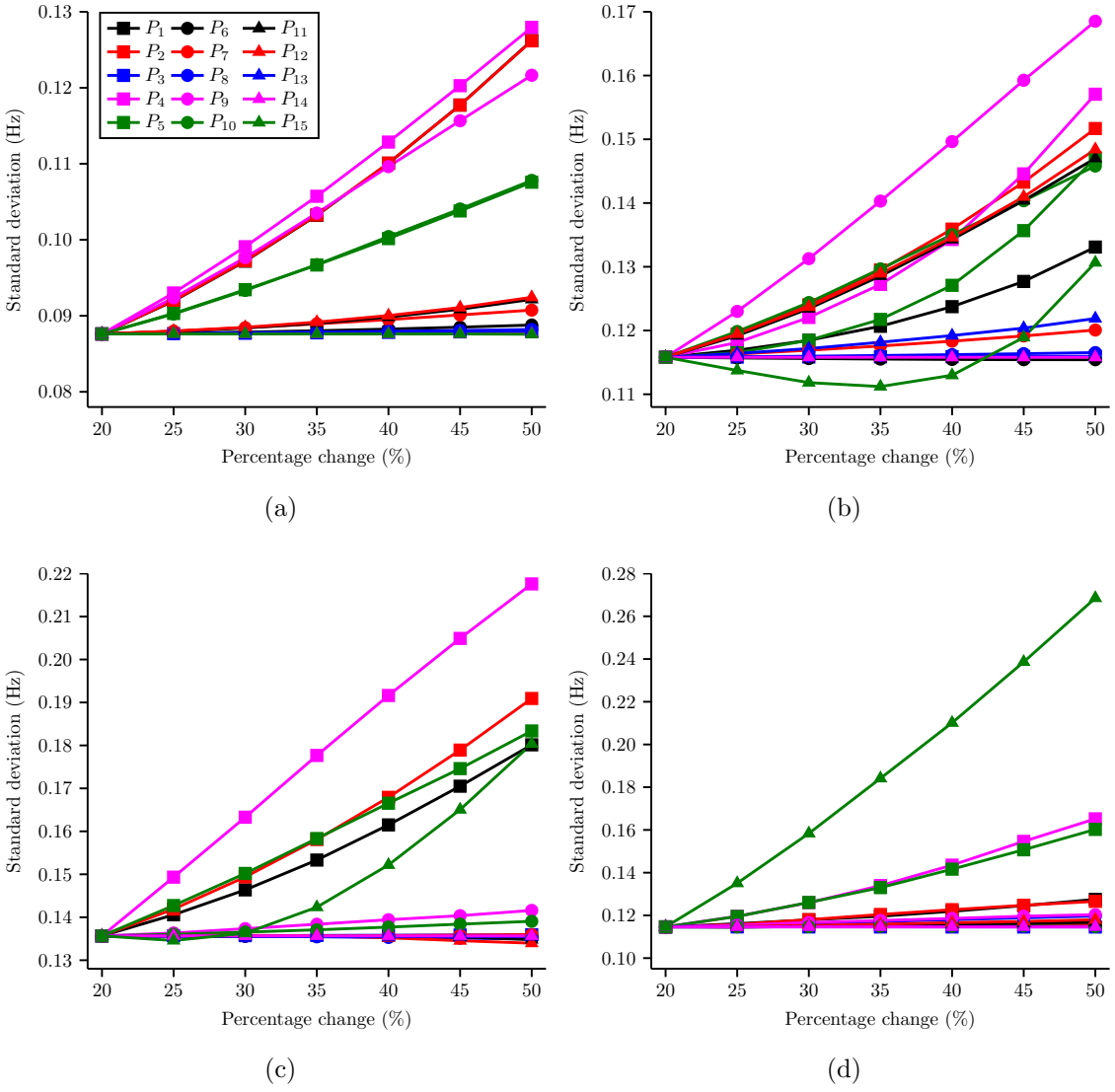

Fig. 11. Standard deviation of modal frequencies of the Beichuan River Bridge versus percentage change in uncertainty: (a) f_1, (b) f_2, (c) f_3 and (d) f_4

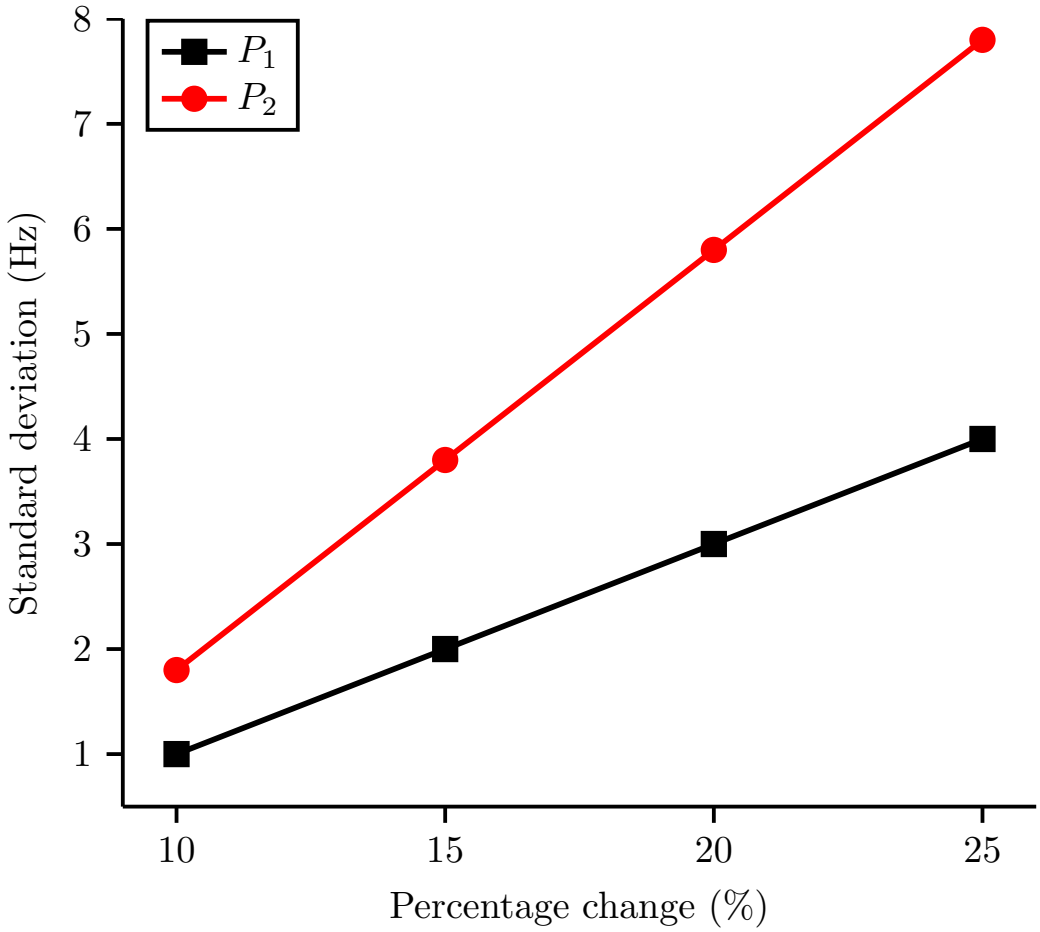

Fig. 12. The use for identical uncertainty bounds explanation.

Tab. 1. Lists of parameters for substructures of the Henghe bridge.

No.	Parameter	Substructure description
1	E_1	Tubes connecting bridge piers (yellow)
2	E_2	Four main chords constituting main truss (cyan)
3	E_3	Struts between top and bottom chords (blue)
4	E_4	Lateral bracing connecting left and right chords (magenta)
5	E_5	Horizontal bracing connecting left and right chords (green)
6	E_6	Railings including railing posts and handrails (red)

Note: Colors in parentheses denote that substructures are demarcated with the associated colors in FEM (Fig. 4).

Tab. 2. Mean and standard deviation of modal frequencies of the Fenghe Bridge (Hz).

Frequency	GP method		MCS		Relative error (%)	
	μ	σ	μ	σ	μ	σ
f_1	4.35140	0.04384	4.35147	0.04408	-0.00161	-0.54446
f_2	5.36819	0.05171	5.36814	0.05200	0.00093	-0.55769
f_3	6.36327	0.05975	6.36331	0.05916	-0.00063	0.99730
f_4	6.71955	0.06298	6.71952	0.06317	0.00045	-0.30078

Note: Relative error=(GP-MCS)/MCS

Tab. 3. Characteristics of parameters of the Beichuan River Bridge.

No.	Parameter	Nominal value
1	Elastic modulus of stell used in hollow tube (P_1)	2.1×10^{11} (Pa)
2	Elastic modulus of concrete filled tubular arch rib (P_2)	4.560×10^{10} (Pa)
3	Moment of inertia of concrete filled tubular arch rib (P_3)	0.0147196 (m^4)
4	Density of concrete filled tubular arch rib (P_4)	2871.14 (kg/m^3)
5	Sectional area of concrete filled tubular arch rib (P_5)	0.4311 (m^2)
6	Elastic modulus of wall above deck (P_6)	2.850×10^{10} (Pa)
7	Density of of wall above deck (P_7)	2500 (kg/m^3)
8	Elastic modulus of deck (P_8)	3.0×10^{10} (Pa)
9	Density of deck (P_9)	2500 (kg/m^3)
10	Thickness of deck (P_{10})	0.25 (m)
11	Elastic modulus of cross girder (P_{11})	3.450×10^{10} (Pa)
12	Moment of inertia of cross girder about major axis (P_{12})	0.0756 (m^4)
13	Sectional area of suspender (P_{13})	0.002494 (m^2)
14	Sectional area of prestressed cable (P_{14})	0.0044428 (m^2)
15	Spring stiffness in lateral direction (P_{15})	5.0×10^5 (N/m)

Tab. 4. Mean and standard deviation of modal frequencies of the Beichuan River Bridge (Hz).

Frequency	GP method		MCS		Relative error(%)	
	μ	σ	μ	σ	μ	σ
f_1	1.71786	0.08778	1.71826	0.08734	-0.02328	0.50378
f_2	2.17624	0.11584	2.17898	0.11476	-0.12575	0.94109
f_3	2.33675	0.13591	2.33710	0.13555	-0.01498	0.26558
f_4	2.65836	0.11926	2.66109	0.11466	-0.10259	4.01186